Available online at www.sciencedirect.com

jmr&t Journal of Materials Research and Technology

journal homepage: www.elsevier.com/locate/jmrt

Original Article

First-principles calculations to investigate mechanical, thermoelectric and optical performance of inorganic double perovskites Rb_2AgAlZ_6 (Z = Br, I) for energy harvesting

Abeer Mera [a,b,**], *Taharh Zelai* [c], *Syed Awais Rouf* [d,*], *Nessrin A. Kattan* [e], *Q. Mahmood* [f,g]

[a] *Physics Department, College of Arts and Science, Wadi Addawasir, Prince Sattam Bin Abdulaziz University, 11991, Saudi Arabia*

[b] *Physics Department, Faculty of Science, Kafrelsheikh University, Kafrelsheikh, 33516; Egypt*

[c] *Department of Physics, Faculty of Science, Jazan University, Jazan, Saudi Arabia*

[d] *Department of Physics, Division of Science and Technology, University of Education, Lahore, Pakistan*

[e] *Departmet of Physics, College of Science, Taibah University, Madina, Saudi Arabia*

[f] *Basic and Applied Scientific Research Center, Imam Abdulrahman Bin Faisal University, P. O. Box 1982, Dammam, 31441, Saudi Arabia*

[g] *Department of Physics, College of Science, Imam Abdulrahman Bin Faisal University, P. O. Box 1982, Dammam, 31441, Saudi Arabia*

ARTICLE INFO

Article history:
Received 23 February 2023
Accepted 19 April 2023
Available online 24 April 2023

Keywords:
Density functional theory
Solar cells and energy harvesting
Figure of merit
Thermal performance
Ductile nature

ABSTRACT

The clean and green energy is a merging technology of advanced era to achieve the demands of energy requirements. For this purpose, the double perovskites Rb_2AgAlZ_6 (Z = Br, I) are explored comprehensively in terms of optical, mechanical, thermoelectric, and thermodynamic characteristics. The stability of structures, elastic and thermodynamic have been ensured through tolerance factor, Born Criteria, and formation energy. The elastic constants of cubic symmetry are analyzed to distinguish ductile/brittle nature, anisotropy, Harness, minimum lattice thermal, conductivity, melting and Debye temperatures. The anions (Br, I) modified the band gaps (2.60, 1.08) eV which turned the absorption of light energy from ultraviolet to visible portion of spectrum. The absorption band of Rb_2AgAsI_6 in the energy range 1.7eV–3.4 eV is particularly significant for solar cells. The large Seebeck coefficient, and electrical conductivity while particularly low lattice thermal conductivity has been increased the figure of merit. The large figure of at low temperature open the new finding roots for realization of these DPs for thermoelectric and other energy applications.

* Corresponding author.
** Corresponding author.
E-mail addresses: awais.physicist@gmail.com (S.A. Rouf), a.mera@psau.edu.sa (A. Mera).

https://doi.org/10.1016/j.jmrt.2023.04.169

1. Introduction

The global economic evolution has increased the human standard of life due to the advent of modern technologies [1–3], which require continuous energy supply and ecological safety [4,5]. The existing energy sources are hazardous to the environment and are quickly depleting [6,7]. Therefore, various renewable energy sources i.e., wind energy [8], hydro power [9], photovoltaic [10] and thermoelectric energy [11] are being widely studied as alternatives to the existing energy sources. Thermoelectric phenomenon is eco-friendly and does not require any mechanical motion of its components [12,13]. A lot of heat energy generated from a variety of modern equipment is wasted [72]. Despite of the fact that thermoelectric phenomenon is being employed since long time, but limited energy conversion efficiency is the main problem [14]. The energy conversion efficiency is termed as the dimensionless figure of merit ZT ($ZT = S^2\sigma T/K$, where S is Seebeck coefficient, is electrical conductivity, while K is thermal conductivity that is equal to lattice K_l and electronic K_e parts) [15]. For attaining maximum ZT, as evident from the expression, thermal conductivity should be as small as possible, but numerator should be high [16]. However, Seebeck coefficient S, which expresses potential drops due to the thermal gradients is linked inversely with the electrical conductivity σ [17]. High S values express insulating nature, while high σ depict metallic character. Due to this, a careful selection of materials exhibiting optimized values of S and σ is of prime significance to exhibit maximum ZT [18]. Generally, narrow band gap semiconductors have appeared as of high potential to exhibit higher ZT [19,20].

Narrow band gap materials are also attractive for infrared photo-detections [21,22] and for field-effect transistors (FET) to exhibit doping induced switching of the ambipolar transport of majority carriers [23]. Although Pb based narrow band gap perovskites exhibit higher photovoltaic energy conversion efficiency [32], but the toxic nature of the constituent Pb and structural instability limit their commercial applications. Therefore, various strategies have been applied to improve the stability during device fabrication, but a trade-off between stability and efficiency exists [24]. The Pb substitution, in the typical perovskite structure, with trivalent and monovalent cations stabilizes a double perovskite structure [25], but indirect band gap makes it less attractive for the devices involving light emissions [26–28]. Various studies about halide double perovskites and oxides [29,30,72] reveal that generally higher optical band gap is exhibited. For IR detection and best thermoelectric performance, narrow band gap double perovskites are required either by designing novel strategies to suppress the intrinsic optical band gaps or by intentionally inducing indirect-to-direct band gap transitions in intrinsically narrow and indirect band gap materials [31–33]. A direct bandgap double perovskite, $Cs_2AgInCl_6$, have been investigated theoretically to reveal the Cu doping effects on the structural and optoelectronic properties. Increasing Cu doping resulted increased photo-absorption coefficient and optical conductivity that indicated suitability for photovoltaics, solar cells, and optoelectronic applications [34]. The double perovskites are vastly studied for magnetic and thermoelectric properties through DFT approach like Ba_2FeMoO_6, Dy_2CoMnO_6 [35,36].

$X_2CuInCl_6$ (X = K, Rb, Cs) halide double perovskites have been reported as stable [37]. The direct energy band gap of Rb2CuInCl6 has been reported as 1.36 eV, which is closer to the optimal value 1.34 eV required to exhibit higher efficiency [38]. The existing literature about Ag–Al based Double perovskites halides Rb_2AgAlZ_6 (Z = Br, I) is very limited. In this study, we present the density functional theory (DFT) based analysis of the thermoelectric, mechanical, and optical behaviors of Rb_2AgAlZ_6 (Z = Br, I) to reveal the potential device applications in wasted heat to electricity conversion and optical detections, respectively.

2. Method of calculations

The DFT is the most versatile approach to solving the materials before realizing them for practical applications. The tool provides the complete information about the characteristics of different materials before realizing them for practical manufacturing [39–44]. In this regard, the Wien2 K code and FP-LAPW method are employed to execute the computations of Rb_2AgAlZ_6 (Z = Br, I) [45,46]. The Murnaghan's equations are incorporated through PBEsol to evaluate the optimized lattice and energy of studied system [47]. The PBEsol has been assess the structural related parameters accurately but the band gaps and electronics are remained miscalculated. Therefore, TB-mBJ potential has been used to calculate the band gaps because it is very simple and precise. Its exactness is equivalent to HSE06, Hybrid functional but TB-mBJ consume less computational time [48]. To find the optical properties and electronic structures for thermoelectric parameters, we have applied PBEsol and TB-mBJ package. Furthermore, the $\ell_{max}/G_{max}/R_{MT} \times K_{max}$ factors which demonstrate the angular momentum, Gaussian factor and muffin-tin sphere to wave factor multiplication are taken as 10.0/14.0/8.0, respectively. The convergence of charge/energy are essentially important for the accuracy of calculated results. Therefore, the high K-mesh of 20 × 20 × 20 has been executed for convergence of energy (10^{-4}Ry). The BoltzTrap and ShengBTE codes are applied for thermoelectric and lattice factors calculations [49,50].

3. Results and discussion

3.1. Structural properties

The cubic structures of DPs Rb_2AgAlZ_6 (Z = Br, I) is the combinations of two simple perovskites structures which have space group Fm $\bar{3}$ m (225). Fig. 1, left side show the arrangement of atoms of Rb, Ag, Al, and Br/I in closed pack cubic structure. The central spacing of Ag and Al based octahedrons are occupied by Rb atoms. On the right side of Fig. 1, the polyhedral shape of structure clearly shows the formations of octahedrons which are split up by 6-fold numbers of Br/I.

The positioned atoms of Ag octahedra (blue color), and Al octahedra (red color) are surrounded by Z atoms. The (Rb, Ag, Al,

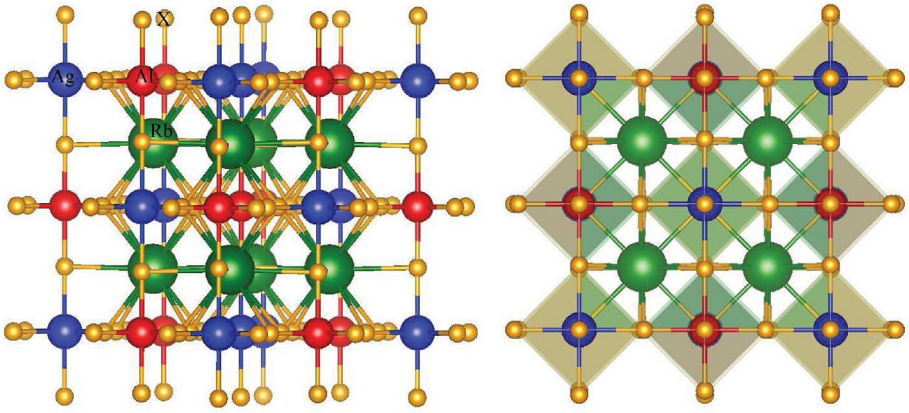

Fig. 1 – Crystal structure in atomic (left) and polyhedral (right) of Rb_2AgAlZ_6 (Z = Br, I) [Rb (green), Ag (blue), Al (red) and Z (yellow) color atoms].

and Z) atoms contained the Wyckoff sites (4(a, b), 8 (c, 3e) [51]. The lattice constant (a_0) of cubic structures are optimized and found the other ground state factors by Murnaghan's equation of states. The value of a_0 is higher for I than Br because of higher ionic radius of I than Br. In contrast, the bulk modulus obtained from optimization, decreases from Br to I. Furthermore, the initial basic test of formation energy has been executed to confirm the existence of studied DPs through relation

$$\Delta H_f = E_{Total}\left(Rb_lAg_mAl_nZ_o\right) - lE_{Rb} - mE_{Ag} - nE_{Al} - oE_Z \quad (1)$$

The individual energies (E_{Rb}, E_{Ag}, E_{Al} and E_Z) of (Rb, Ag, Al and Z) atoms are subtracted from the total energy $E_{Total}(Rb_lAg_mAl_nZ_o)$ of compounds Rb_2AgAlZ_6. The negative sign of ΔH_f provide the confirmation of thermodynamic existence of studied DPs (See Table 1) [52]. Furthermore, the existence of structures is computed by the ratio of ionic radii of elements in the structures through the relation of tolerance factor

$$t_F = \frac{r_{Rb} + r_Z}{r_B + r_Z} \quad (2)$$

Where B is the average ionic radius of Ag and Al at octahedral sites, and (r_{Rb}, r_B and r_Z) are the ionic radii of elements (Rb, Ag/Al, Z). These radii of elements are calculated from the execution of Xcrysden software from the improved structures. The computed values of t_F are in the range of 0.94–1.0 which show the structures are stable (See Table 1) [53].

Table 1 – The lattice and optical parameters of Rb_2AgAlZ_6 (Z = Br, I).

Parameter	$Rb_2AgAlBr_6$	Rb_2AgAlI_6
a_o (Å)	11.01	11.77
B_o(GPa)	22.50	20.65
H_f(eV)	−1.57	−1.23
T_f	0.98	0.88
E_g(eV)	2.60	1.08
$\varepsilon_1(0)$	3.00	3.69
n(0)	1.74	1.92
R(0)	0.073	0.099
m_e^*	$0.20m_0$	$0.27m_0$
m_h^*	$0.31\ m_0$	$0.37\ m_0$

3.2. *Mechanical characteristics*

The elastic constants and mechanical characteristics of studied DPs are investigated by Chapin method. For cubic crystal structures three independent constants (C_{11}, C_{12} & C_{44}) explore all the necessary information about mechanical and thermodynamical characteristics. The computed elastic constants satisfy the Born conditions of stability $C_{44} > 0$, bulk modulus is between C11 and C12, and C_{11}–C_{12}>0 [54]. The bulk modulus (B) is degcreases from Br to I while Young (Y) and shear modulus (G) increases because of different anisotropic orientation. The ratio of B and G (Pugh's condition) is greater than >1.75 for ductile materials while the Possion condition (υ) for ductile behavior is > 0.26. The values in Table 2 show the studied DPs are ductile [55]. The comparative analysis show the $Rb_2AgAlBr_6$ is more ductile than Rb_2AgAlI_6. Furthermore, anisotropy factor (A) has been computed whose value for isotropic character is unity and changes from this value considered as anisotropic behavior. The calculated reports in Table 2 show the

Table 2 – Elastic and thermodynamic paramters of Rb_2AgAlZ_6 (Z = Br, I).

Parameters	$Rb_2AgAlBr_6$	Rb_2AgAlI_6
C_{11} (GPa)	41.27	39.02
C_{12} (GPa)	13.52	11.20
C_{44} (GPa)	5.27	10.59
B (GPa)	22.77	20.47
G (GPa)	7.86	11.81
E (GPa)	21.15	29.72
B/G	2.90	1.76
Y	0.35	0.26
A	0.38	0.76
V_ℓ (Km/s)	3.03	2.90
V_t (Km/s)	1.47	1.66
V_m (Km/s)	1.65	1.85
Θ_D (K)	154	165
T_m (K)	796	783
H_a (GPa)	2.78×10^6	6.65×10^6
K_{min} (W/mK)	0.129	0.122
K_{min} [100] (W/mK)	0.125	0.121
K_{min} [110] (W/mK)	0.185	0.156
K_{min} [111] (W/mK)	0.138	0.123

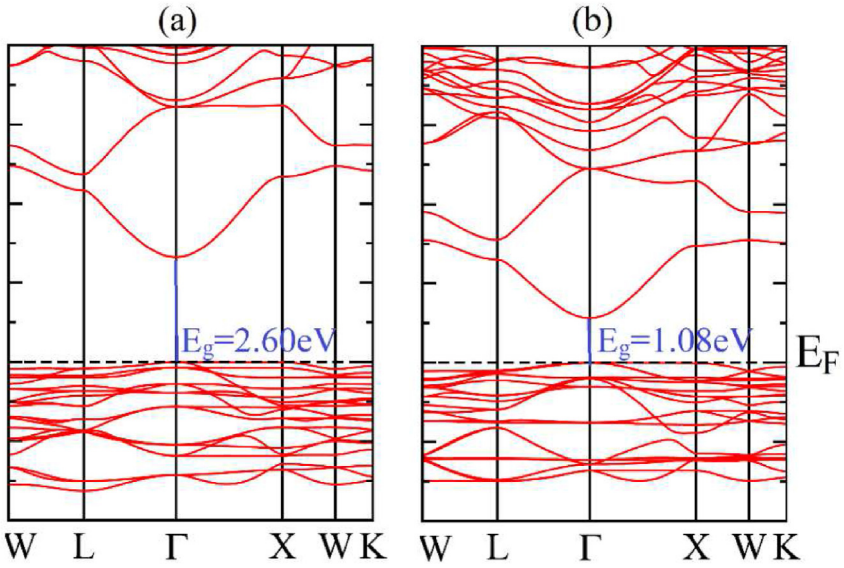

Fig. 2 – The band structures along high symmetry of (a) $Rb_2AgAlBr_6$ and (b) Rb_2AgAlI_6.

$Rb_2AgAlBr_6$ is hihgly anisotropic and Rb_2AgAlI_6 is less anisotropic because of deviation from unity. For the calculations of Debye temperature (θ_D), we have solved first the longitudinal (V_ℓ) and transverse (V_t) parts of sound velocity through Navier equation of states to average their values (υ_m) [56,57]. Therefore, Debye teperautre has been computed by formula,

$$\theta_D = \frac{h}{k_B}\left[\frac{3nN_A\rho}{4\pi M}\right]^{\frac{1}{3}} \upsilon_m \quad (3)$$

Here (M, ρ, N_A) are constants. The calculated Θ_D has been presented in Table 2, which has reasonable values. The Θ_D provide information about specific heat capcity which resist the thermal changes in the materials [58,59].

The melting temperature is an important paramter which decide the feasibility of the material for device application. Here it is calculated from the relation $T_m = 553 + 5.91\ C_{11}$/GPa. The large values of T_m (796, 783)K for studied DPs are ensured that these materials are suitable for device fabrications at room temperature. The Tm of $Rb_2AgAlBr_6$ is higher than Rb_2AgAlI_6 because of tough bonding in the earlier. The hardness is another paramter which ensure the reliability of the materials which is calculated by relation,

$$Hv = 0.92(G/B)^{1.137}G^{0.708} \quad (4)$$

The large values of Hv show endurance against the variations in the shape of the materials. Its values are very large for the studied DPs which ensure their importance for devices [60]. The values of Hv presented in Table 2, show the Rb_2AgAlI_6 is harder than $Rb_2AgAlBr_6$. Furthermore, the minimum value of thermal conductivity (k_{min}) has been reported through the Cahill formula [64]

$$k_{min} = \frac{k}{2.48}(n_b)^{\frac{2}{3}}(\upsilon_l + 2\upsilon_t) \quad (5)$$

Here n_b show the atom per unit cell. The calculated values of k_{min} has been presented in Table 2 which have enormously

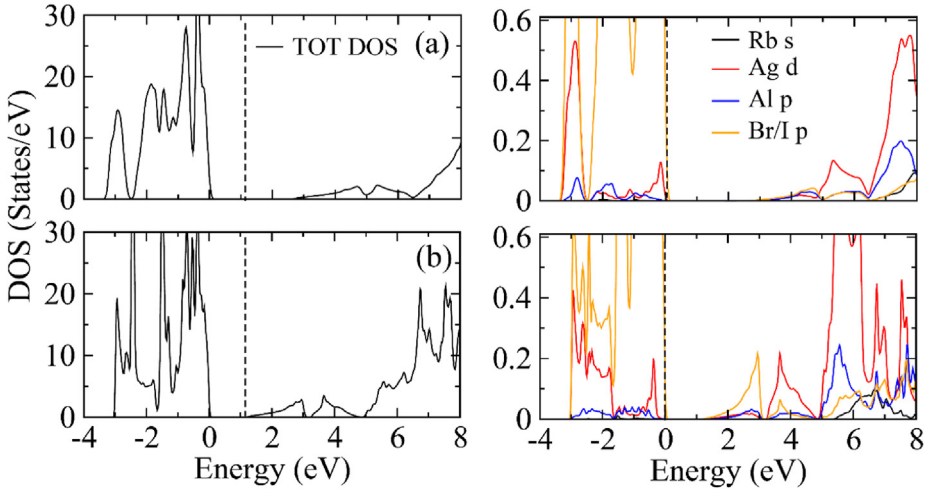

Fig. 3 – The DOS of compounds (left side) and separate elements Rb, Ag, Al, Br/I (right side) of (a) $Rb_2AgAlBr_6$ and (b) Rb_2AgAlI_6.

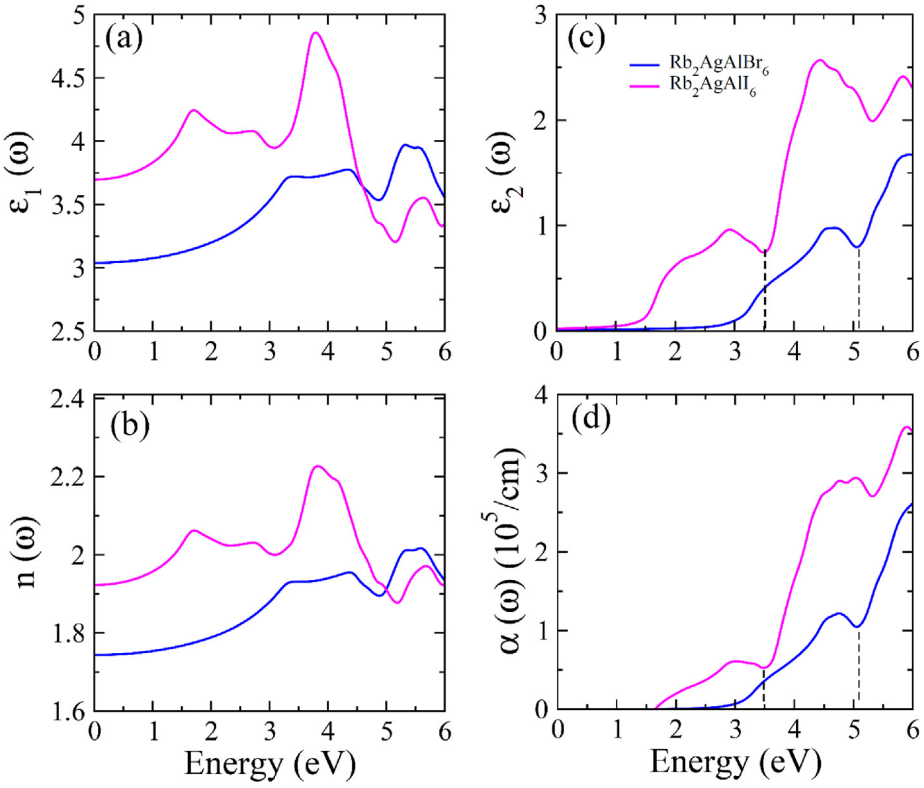

Fig. 4 – (a, b) Representation of dispersion factors $\varepsilon_1(\omega)$ & n(ω), and (c, d) absorption factors $\varepsilon_2(\omega)$ & α (ω) for Rb_2AgAlZ_6 (Z = Br, I).

low values. Therefore, small values of k_{min} increases the performance of the materials.

3.3. *Electronic properties*

The band structures are plotted in Fig. 2 (a, b) which mention the nature of examined materials. The BS ensure the direct band gaps at Γ direction which numerical values 2.60 eV, and 1.08 eV for $Rb_2AgAlBr_6$, and Rb_2AgAlI_6, respectively. The direct band gap and inter-band transitions increase the expressively valuable features which boost the scope of materials for solar cells. The band gap decreases from 2.60 eV to 1.08 eV from Br to I because of increasing the ionic radius of halide ions at the center of octahedrons. This increase in the size of halide ions lessens the gap between valence and conduction bands. It is also noted from BS the states are flat and large in number in VB while states are curved and less in number in the CB. Therefore, the effective mass.

m_h^* are larger than the electrons m_e^* which confirm the p-type character of these materials (See Table 1).

Moreover, the density of states is plotted in Fig. 3 (a, b) which illustrate the distribution of electrons of Rb_2AgAlZ_6, Rb, Ag, Al, and Z atoms. The lift side of TDOS show the identical behavior as BS. The electrons of Rb atom exist in the deep region, away from the VB and CB which do not contribute significantly in the transition mechanism. However, the d-states electrons of Ag, p-states electrons of Al and Br/I are responsible for the transitions and recombination of electrons. At −2.5 eV and 6 eV the contribution of 3d-Ag is maximum and CB minima is formed by p-Br/I therefore, electrons also leap inside the halide ions and 3d-Ag states.

3.4. *Optical properties*

The solar cells and photovoltaic characteristics of materials depends the band gap, energy absorption and efficiency of materials to convert light into electrical energy. The direct band gaps are appreciably essential because direct transformation of electrons between VB and CB bands avoid the phonons emission and increase the reliability of optical device. In present article, the optical behavior of Rb_2AgAlZ_6 (Z = Br, I) has been elaborated in terms of dielectric constants $\varepsilon_1(\omega) + i\varepsilon_2(\omega)$, where its real section has been denoted by $\varepsilon_1(\omega)$ and fictional section by $\varepsilon_2(\omega)$. The $\varepsilon_1(\omega)$ classify the distribution and divergence while $\varepsilon_2(\omega)$ specify the decrease in the light strength when it pass through the materials. This is also measured in terms of attenuated of energy by the materials are absorbed part [30,61–65]. Here the complete set optical parameters are explained in Figs. 4 and 5 (a-d). The zero-energy limit of $\varepsilon_1(\omega)$ and band gaps are related through the Penn's equation $\varepsilon_1(0) \approx 1 + (\hbar\omega_p/E_g)^2$ [66]. The calculated $\varepsilon_1(\omega)$ and E_g are shown in Table 1 which are exactly satisfy the Penn's relation. The zero energy numbers 3.0/3.69 increase with growing energy and attain the first peak at 3.3/1.8 eV and second peaks at 5.5/3.8 eV for Br/I based DPs (See Fig. 4a). At these peaks, resonance frequency fully polarized the light and after that it drops to minimum. The substitute of I ions in place of Br increases the dispersion which shows the halide

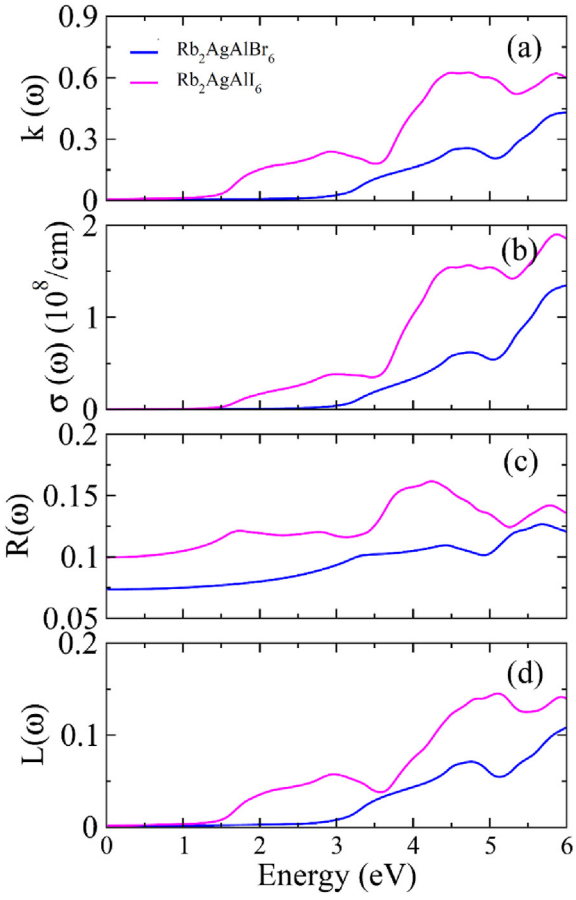

Fig. 5 – (a, b) Representation of Ext. coeff and Opt. conductivity $k_1(\omega)$ & $\sigma(\omega)$, and (c, d) Reflection and loss factors R(ω) & L (ω) for Rb_2AgAlZ_6 (Z = Br, I).

ions have significant impact on the optical characteristics. The divergence of light energy can also be understood from refractive index n(ω) (See Fig. 4b) which is the replica of $\varepsilon_1(\omega)$. There zero energy values are related through $n_0^2 = \varepsilon_1(0)$ [67]. The coherence between $\varepsilon_1(\omega)$ and n(ω) show the similar trends of graphs with growing energy which is important for the accuracy of results.

The Kramer–Kronig relation [68] has been integrated to solve the dielectric constants whose imaginary contribution is represented by $\varepsilon_2(\omega)$ as shown in Fig. 4c. It measures the absorption of light energy in the regions from 3.1 to 5.1 eV, and 1.7–3.4 eV for $Rb_2AgAlBr_6$, and Rb_2AgAlI_6, respectively. The absorption band of Rb_2AgAlI_6 exists in the visible light range which is suitable for solar cells and $Rb_2AgAlBr_6$ is appropriate for optoelectronic devices in ultraviolet section. Furthermore, the optical band gaps (2.60, 1.08) eV are determined by tangent lines of the curves which are consistent with band gaps acquired from BS. In same way, the absorption coefficient α (ω) also describe the decrease of light energy when it passes through materials. The computed values of α (ω) are portrayed in Fig. 4d. The decrease in energy per centimeter (decay rate) is similar as represented in the graph of $\varepsilon_2(\omega)$.

Furthermore, refraction of light energy has been distributed in two parts whose imaginary section is represented as extinction coefficient k (ω), is also represented the decay of light energy. Its graphed values in Fig. 5a also consolidate the pattern of α (ω) and $\varepsilon_2(\omega)$. For the complete analysis of optical parameters, the conduction of electrons σ (ω) is generated by the absorption of light energy as plotted in Fig. 5b. The trends of σ (ω) are equivalent to absorption parameters because the free electrons depend upon the energy absorbed by the materials.

The incident light energy on the materials is distributed in transmission, reflection, and absorption. The reflection of light energy during interaction with materials surface has been presented in Fig. 5c. R(0) has been noted 0.073 and 0.099 for $Rb_2AgAlBr_6$, and Rb_2AgAlI_6, respectively. Its value remains in the range from zero to 0.2 in visible range. Furthermore, a fraction of light energy also lost in the form of dispersion, and other losses. Therefore, the loss of optical energy L(ω) has been graphed in Fig. 5d which shows the loss of energy for studied materials is very small. The major part of incident energy is absorbed by the materials. On the base of complete analysis of optical behavior of these DPs, it is observed the Rb_2AgAlI_6 is important for solar cells.

3.5. *Thermoelectric properties*

The waste heat can also be utilized for energy consumption through thermoelectric generators. The efficiency of thermoelectric materials is analyzed by the figure of merit which is evaluated through formula $\sigma S^2/k$. Here "S" is the Seebeck coefficient which is measured from the potential gradient between dissimilar metals, "σ" is electrical conductivity which determine the flow of carriers, and "κ" is the thermal conductivity measured from lattice vibration. For optimum performance, the S and σ are large while the κ should be least [69–76]. In this article, the transport characteristics, of studied DPs are computed by BoltzTrap code in the temperature span 100–600 K as depicted in Fig. 6 (a-d) and Fig. 7 (a, b). The σ represented in Fig. 6a, show the linear increases in its values with growing temperature from 100 to 600 K because the increasing temperature creates more electrons and holes. The σ for Rb_2AgAlI_6 is larger than $Rb_2AgAlBr_6$ because I have a greater number of free electrons as compared to Br.

The κ is involved from electrons as well as from the lattice vibration. The contribution from electrons is represented by κ_{el} and from phonons, it is denoted by κ_{ph}. The contribution of κ_{ph} has been dropped because of heavy calculations and constraints on BoltzTraP code. Therefore, calculated κ_{el} has been graphed in Fig. 6b for the studied DPs. The observation of graphs ensures the similar type of behavior as σ. The κ_{el} is also greater for Rb_2AgAlI_6 as compared to $Rb_2AgAlBr_6$ because more electrons Rb_2AgAlI_6 and greater ionic radius of iodide than bromide. For the analysis of performance, the ratio κ_{el}/σ has been calculated which confirm the σ is 10^5 greater than κ_{el} which make them significantly importance materials for thermoelectric generators [77].

The potential variation between the different metals against the temperature change has been recorded in terms of Seebeck coefficient (S). The plotted graphs of S for $Rb_2AgAlBr_6$ and Rb_2AgAlI_6 are shown in Fig. 6c which show increases in values from 0.195/0.218 mV/K to 0.178/0.182 mV/K as T increases from 100 to 600 K. This decrease in S is due to increase in intensity of electrons (σ). In DPs, the large values of S play a

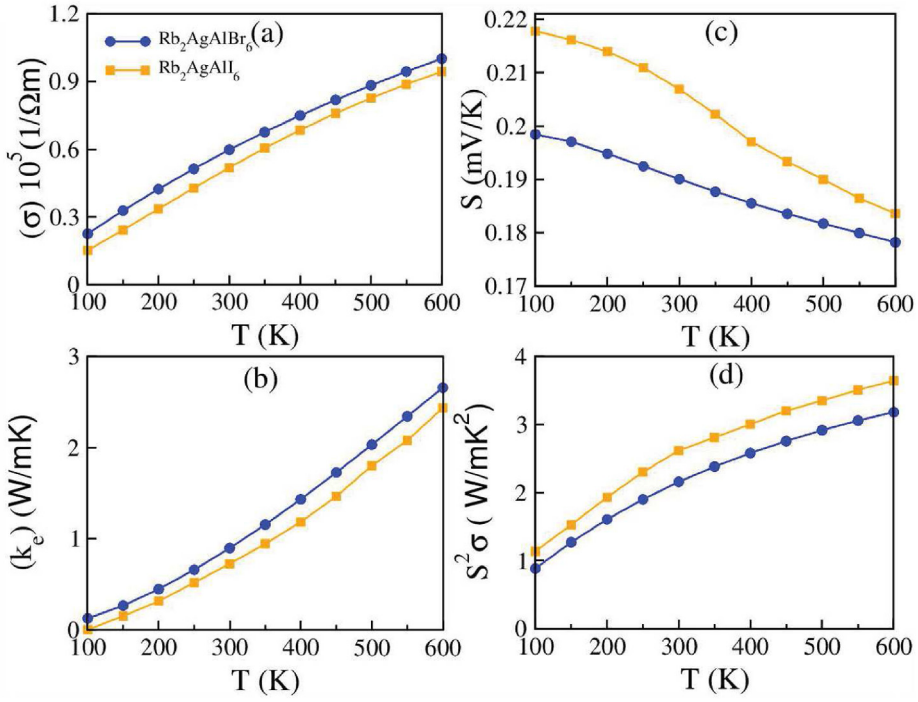

Fig. 6 – (a, b) Representation of conduction factors (σ & κ_e) and (c, d) Seebeck coeff. and power factors (S & σS^2) for Rb_2AgAlZ_6 (Z = Br, I).

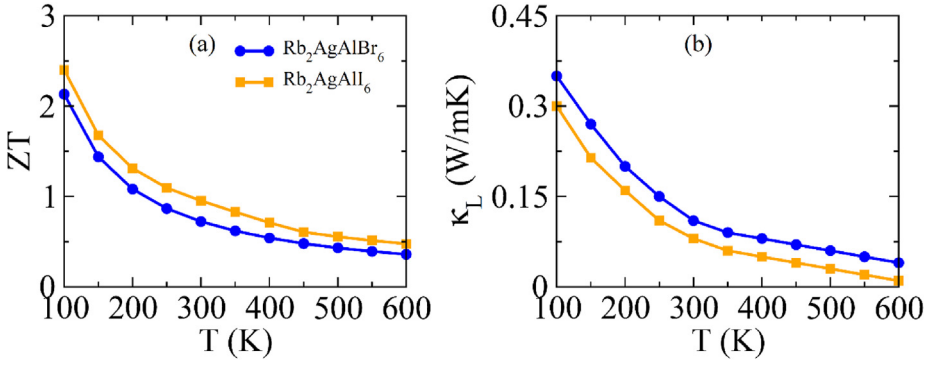

Fig. 7 – (a) Representation of performance factors (ZT) and (b) lattice vibration factor (κ_L) for Rb_2AgAlZ_6 (Z = Br, I).

significant role to boost the thermoelectric performance (TP). Therefore, the power factor (PF) has been computed as (σS^2) with out the effect of κ, to understand the TP of studied DPs. The PF increases from 0.9/1.1 to 3.2/3.6 W/mK^2 with growing T from 100 to 600 K (See Fig. 6d).

However, TP can not be identified without including the κ contribution. Therefore, the ZT has been graphed in Fig. 7a which provide accurate merit of scale for TP. Its values are high at low and even at room T which assured the importance of these DPs for thermoelectric generators. From the studied DPs, the Rb_2AgAlI_6 is comparatively better because of higher values of ZT than $Rb_2AgAlBr_6$ which is approximately unity at 300 K. The κ_ℓ is the most important factor to influence the ZT. Therefore, it has been included in ZT and has also been plotted separately in Fig. 7b.

For excellence performance, its values should be lowest to enhance the ZT. Some thermoelectric players are cited below to compare the κ_ℓ of studied DPs. At room temperature, our studied DPs have 0.14 and 0.12 W/mK which is very less as compared to 0.15/1.24/2.60 W/mK for Cs_2PdI_6/Bi_2Te_3/GeTe [78–81].

4. Conclusions

Comprehensively, the DPs Rb_2AgAlZ_6 (Z = Br, I) are addressed solar cells and transport applications by the analysis of optical, mechanical, thermoelectric, and thermodynamic characteristics. The structures of studied DPs are stable because of ideal values of tolerance factor, Born mechanical conditions,

and negative formation energies. From mechanical criteria, it is also found the ductile nature, ultralow minimum lattice conductivity, Large melting, and Debye temperatures. The BS analysis show the direct transitions and band gaps between VB and CB. The absorption bands are invisible span for Rb_2AgAlI_6, and ultraviolet region for $Rb_2AgAlBr_6$. Furthermore, studied materials are completely polarized, and have least losses of energy which boost their applications for solar cells. In addition, to above thermoelectric efficiency has scrutinized in terms of ZT. It shows the large values of ZT at low temperature. The Rb_2AgAlI_6 has unity value at room temperature which is highly appreciated for transport applications. Finally, our findings of DFT will provide inclusive knowledge to the experimental researchers to realize them for solar cells.

Conflict of interest

The author declares no competing financial interests.

Declaration of competing interest

The authors declare that they have no known competing financial interests or personal relationships that could have appeared to influence the work reported in this paper.

Acknowledgement

The authors extend their appreciation to the Deputyship for Research & Innovation, Ministry of Education in Saudi Arabia for funding this research work through the project number (IF2/PSAU/2022/01/22718).

REFERENCES

[1] Ramesh PL. Impact of Technology in Human Life. Global Journal for Research Analysis 2017;06:09.
[2] Steinberger JK, Rao ND. Providing decent living with minimum energy: A global scenario. Glob Environ Change 2020;65:102168.
[3] Afshin A, Babalola D, Mclean M, Yu Z, Ma W, Chen CY, et al. Information technology and lifestyle: a systematic evaluation of internet and mobile interventions for improving diet, physical activity, obesity, tobacco, and alcohol use. J Am Heart Assoc 2016;5:e003058.
[4] Perez M, Perez R. A fundamental look at supply side energy reserves for the planet. Solar Energy Advances 2022;2:100014.
[5] Voulvoulis N, Burgman MA. The contrasting roles of science and technology in environmental challenges. Crit Rev Environ Sci Technol 2019;49:1079–106.
[6] Asghar MM, Wang Z, Wang B, Zaidi SAH. Nonrenewable energy-environmental and health effects on human capital: empirical evidence from Pakistan. Environ Sci Pollut Res 2020;27:2630–46.
[7] Awodumi OB, Adewuyi AO. The role of non-renewable energy consumption in economic growth and carbon emission: evidence from oil producing economies in Africa. Energy Strategy Rev 2020;27:100434.
[8] Kumar A, Khan M, Pandey B. Wind energy: a review paper. Gyancity Journal of Engineering and Technology 2018;4:29–37.
[9] Kaunda C, Kimambo C, Nielsen T. Hydropower in the context of sustainable energy supply: a review of technologies and challenges. ISRN Renewable Energy 2012;1:730631.
[10] Zelai T, Rouf SA, Mahmood Q, Bouzgarrou S, Amin MA, Aljameel AI, et al. J Mater Res Technol 2022;16:631–9.
[11] Chen HN, Xiang SS, Li WP, Liu HC, Zhu LQ, Yang SH. Inorganic perovskite solar cells: a rapidly growing field. Sol. RRL 2018;2:23.
[12] Al-Muhimeed TI, Shafique A, AlObaid AA, Morsi M, Nazir G, Al-Anazy MM, et al. New lead-free double perovskites X_2GeI_6 (X = K, Rb, Cs) for solar cells. and renewable energy as an alternate of hybrid perovskites 2021;45(13):19645–52.
[13] Eperon GE, Leijtens T, Bush KA, Prasanna R, Green T, Wang J, et al. Perovskite-perovskite tandem photovoltaics with optimized band gaps. Science 2016;354:861–5.
[14] Bidai K, Ameri M, Amel S, Ameri I. First-principles calculations of pressure and temperature dependence of thermodynamic properties of anti-perovskite $BiNBa_3$ compound. Chin J Phys 2017;55:2144–55.
[15] Zhou L, Xu YF, Chen BX, Kuang DB, Su CY. Synthesis and photocatalytic application of stable lead-free $Cs_2AgBiBr_6$ perovskite nanocrystals. Small 2018;14:1703762.
[16] Hegde GS, Prabhu AN, Chattopadhyay MK. Improved electrical conductivity and power factor in Sn and Se co-doped melt grown Bi_2Te_3 single crystal. J Mater Sci Mater Electron 2021;32:24871–88.
[17] Jacob J, Rehman U, Mahmood K, Ali A, Ashfaq A, Amin N, et al. Simultaneous enhancement of Seebeck coefficient and electrical conductivity in ZnSnO by the engineering of grain boundaries using post annealing. Phys Lett 2021;388:127034.
[18] Geisz JF, Steiner MA, Jain N, Schulte KL, France RM, McMahon WE, et al. Building a six-junction inverted metamorphic concentrator solar cell. IEEE J Photovoltaics 2018;8(2):626–32.
[19] Li ZZ, Xu QC, Sun QD, Hou ZF, Yin WJ. Thermodynamic stability landscape of halide double perovskites via high-throughput computing and machine learning. Adv Funct Mater 2019;29:1807280.
[20] Zhang YY, Chen SY, Xu P, Xiang H, Gong XG, Walsh A, et al. Intrinsic instability of the Hybrid halide perovskite semiconductor $CH_3NH_3PbI_3$. Chin Phys Lett 2018;35:036104.
[21] Guo Q, Pospischil A, Bhuiyan M, Jiang H, Tian H, Farmer D, et al. Black phosphorus mid-infrared photodetectors with high gain. Nano Lett 2016;16:4648–55.
[22] Yuan H, Liu X, Afshinmanesh F, Li W, et al. Polarization-sensitive broadband photodetector using a black phosphorus vertical p-n junction. Nat Nanotechnol 2015;10:707–13.
[23] Li L, Yu Y, Ye G, Ge Q, Ou Q, Wu H, et al. Black phosphorus field-effect transistors. Nat Nanotechnol 2014;9:372–7.
[24] Pak Y, Mitra S, Alaal N, Xin B, Lopatin S, Almalawi D, et al. Dark Current reduction accompanied photocurrent enhancement in p-type MnO quantum-dot decorated n-type 2D-MoS2-based photodetector. Appl Phys Lett 2020;116(11):112102.
[25] Ajia IA, Edwards PR, Liu Z, Yan JC, Martin RW, Roqan IS. Excitonic localization in AlN-rich $Al_xGa_{1-x}N/Al_yGa_{1-y}N$ multi-quantum-well grain boundaries. Appl Phys Lett 2014;105(12):122111.
[26] Mitra S, Pak Y, Xin B, Almalawi DR, Wehbe N, Roqan IS. Solar-blind self-powered photodetector using solution-processed amorphous core–shell gallium oxide nanoparticles. ACS Appl Mater Interfaces 2019;11(42):38921–8.

[27] Reshak AH, Abu-Jafar MS, Al-Douri Y. Two symmetric n-type interfaces $SrTiO_3/LaAlO_3$ in perovskite: electronic properties from density functional theory. J Appl Phys 2016;119:245303–10.
[28] Arar R, Ouahrani T, Varshney D, Khenata R. Structural, mechanical, and electronic properties of sodium based fluoroperovskites $NaXF_3$ (X=Mg, Zn) from first-principle calculations. Mater Sci Semicond Process 2015;33:127–35.
[29] Benkabou MH, Harmel M, Haddou A, Yakoubi A. Structural, electronic, optical, and thermodynamic investigations of $NaXF_3$ (X = Ca and Sr): first-principles calculations. Chin J Phys 2018;56:131–44.
[30] Alaal N, Roqan IS. Tuning the electronic properties of hexagonal two-dimensional GaN monolayers via doping for enhanced optoelectronic applications. ACS Appl Nano Mater 2018;2(1):202–13.
[31] Roqan IS, O'Donnell KP, Martin RW, Edwards PR, Song SF, Vantomme A. Identification of the prime optical center in GaN: Eu^{3+}. Phys Rev B 2010;81(8):085209.
[32] Slavney AH, Leppert L, Valdes A, et al. Small-Band-Gap Halide Double Perovskites 2018;57:12765–70.
[33] Slavney AH, Leppert L, Bartesaghi D, Gold-Parker A, Toney MF, Savenije TJ, et al. J Am Chem Soc 2017;139:5015.
[34] Ogunniranye IB, Atsue T, Oyewande OE. Structural and optoelectronic behavior of the copper doped $Cs_2AgInCl_6$ double perovskite: a density functional theory investigation. Phys Rev B 2021;103:024102.
[35] Radja K, Farah BL, Ibrahim A, Lamia D, Fatima I, Nabil B, et al. Investigation of structural, magneto-electronic, elastic, mechanical and thermoelectric properties of novel lead-free halide double perovskite $Cs_2AgFeCl_6$: first-principles calculations. J Phys Chem Solid 2022;167:110795–802.
[36] Gherriche A, Bouhemadou A, Al-Douri Y, Bin-Omran S, Khenata R, Hadi MA. Ab initio exploration of the structural, elastic, electronic and optical properties of a new layered perovskite-type oxyfluoride: $CsSrNb_2O_6F$. Mater Sci Semicond Process 2021;131:105890–900.
[37] Zhao XG, Yang D, Sun Y, Li T, Zhang L, Yu L, et al. Cu-in halide perovskite solar absorbers. J Am Chem Soc 2017;139:6718–25.
[38] Wu Y, Li X, Zeng H. Lead-free halide double perovskites: structure, luminescence, and applications. Small Struct 2021;2:2000071.
[39] Zerarga F, Allali D, Bouhemadou A, Khenata R, Deghfel B, et al. Ab initio study of the pressure dependence of mechanical and thermodynamic properties of GeB_2O_4 (B = Mg, Zn and Cd) spinel crystals. Computational Condensed Matter 2022;32:705–15.
[40] Khireddine A, Bouhemadou A, Maabed S, Bin-Omran S, Khenata R, Al-Douri Y. Elastic, electronic, optical, and thermoelectric properties of the novel Zintl-phase Ba_2ZnP_2. Solid State Sci 2022;128:106893–906.
[41] Belkilali W, Belkharroubi F, Ameri M, Ramdani N. Theoretical investigations of structural, mechanical, electronic, and optical properties of NaScSi alloy. Emergent Materials 2021;4:1465–77.
[42] Souadia Z, Bouhemadou A, Khenata R, Al-Douri Y. Structural, elastic and lattice dynamical properties of the alkali metal tellurides: first-principles study. Phys B Condens Matter 2017;521:204–14.
[43] Boudiaf K, Bouhemadou A, Boudrifa O, Haddadi K. Structural, elastic, electronic and optical properties of LaOAgS-type silver fluoride chalcogenides: first-principles study. J Electron Mater 2017;46:4539–56.
[44] Belhachemi A, Abid H, Al-Douri Y, Sehil M, Bouhemadou A, Ameri M. First-principles calculations to investigate the structural, electronic, and optical properties of $Zn_{1-x}Mg_xTe$ ternary alloys. Chin J Phys 2017;55:1018–31.
[45] Blaha P, Schwarz K, Madsen GKH, Kvasnicka D, Luitz J. Techn. An augmented plane wave+ local orbitals program for calculating crystal properties. 2001.
[46] Schwarz K, Blaha P, Madsen GKH. Electronic structure calculations of solids using the WIEN2k package for material sciences. Comput Phys Commun 2002;147:71.
[47] Petersen M, Wagner F, Hufnagel L, Scheffler M, Blaha P, Schwarz K. Improving the efficiency of FP-LAPW calculations. Comput Phys Commun 2000;126:294–309.
[48] Perdew JP, Burke K, Ernzerhof M. Generalized gradient approximation made simple. Phys Rev Lett 1996;77:3865.
[49] Tran F, Blaha P. Accurate band gaps of semiconductors and insulators with a semi-local exchange-correlation potential. Phys Rev Lett 2009;102:226401.
[50] Madsen GK, Singh DJ. BoltzTraP. A code for calculating band-structure dependent quantities. Comput Phys Commun 2006;175:67.
[51] Mahmood Q, Zelai T, Hassan M, Nazir G, Albalawi H, et al. Study of lead-free double perovskites X_2AgBiI_6 (X = K, Rb, Cs) for solar cells and thermoelectric applications. J Mater Res Technol 2023;22:913–22.
[52] Goldschmidt VM. Die gesetze der krystallochemie. Naturwissenschaften 1926;14:477–85.
[53] Topor L, Navrotsky A, Zhao Y, Weidner DJ. Thermochemistry of Fluoride Perovskites: Heat Capacity, Enthalpy of Formation, and Phase Transition of NaMgF3. J. Sold. Stat. Chem. 1997;132:131–8.
[54] Ji X, Yu Y, Ji J, Long J, Chen J, Liu D. Theoretical studies of the pressure-induced phase transition and elastic properties of BeS. J Alloys Compd 2015;623:304–10.
[55] Roknuzzaman M, Ostrikov K, Wang H, Du A, Tesfamichael T. Towards lead-free perovskite photovoltaics and optoelectronics by ab-initio simulations. Sci Rep 2017;7:14025.
[56] Tariq S, Ahmed A, Saad S, Tariq S. Structural, electronic and elastic properties of the cubic CaTiO3 under pressure: a DFT study. AIP Adv 2015;5:077111.
[57] Nazir G, Rehman A, Hussain S, Algrafy E, Mahmood Q, Mera A, et al. Study of narrow band gap double perovskites $(Sr/Ba)_2BB'O_6$ (B = In, Tl, B' = Sb, Bi) for optical, thermoelectric, and mechanical properties. Mater Today Commun 2022;31:103547.
[58] Anbarasan R, Srinivasan M, Suriakarthick R, Albalawi H, Sundar JK, Ramasamy P, et al. Exploring the structural, mechanical, electronic, and optical properties of double perovskites of Cs_2AgInX_6 (X = Cl, Br, I) by first-principles calculations. J Solid State Chem 2022;310:123025.
[59] Ashiq MGB, Mahmood Q, Haq BU, Flemban TH, Kattan NA, Alshahrani T, et al. The study of electronics, optoelectronics, thermoelectric, and mechanical properties of $Zn/CdSnO_3$ perovskites. Mater Sci Semicond Process 2022;137:106229.
[60] Amin MA, Nazir G, Mahmood Q, Alzahrani J, Kattan NA, Mera A, et al. Study of double perovskites X_2InSbO_6 (X = Sr, Ba) for renewable energy; alternative of organic-inorganic perovskites. J Mater Res Technol 2022;18:4403–12.
[61] Tariq S, Jamil MI, Sharif A, Ramay SM, Ahmad H, Qamar N, et al. Exploring structural, electronic and thermo-elastic properties of metallic $AMoO_3$ (A=Pb, Ba, Sr) molybdates. Appl Phys A 2018;124:44.
[62] Mahmood Q, Nazir G, Bouzgarrou S, Aljameel AI, Rehman A, Albalawi H, et al. Study of new lead-free double perovskites halides Tl_2TiX_6 (X = Cl, Br, I) for solar cells and renewable energy devices. J Solid State Chem 2022;308:122887.
[63] Zelai T, Rouf SA, Mahmood Q, Bouzgarrou S, Amin MA, Aljameel AI, et al. First-principles study of lead-free double perovskites Ga_2PdX_6 (X = Cl, Br, and I) for solar cells and renewable energy. JMRT 2022;16:631–9.

[64] Belhadj H, Ameri M, Abbar B, Moulay N, et al. Optical properties of $(Pb_{1-x}Mn_xS)_{1-y}Fe_y$ materials from first-principles calculations, Chinese. J Phys 2017;55:1032–43.
[65] Al-Douri Y, Ameri M, Bouhemadou A, Batoo Khalid M. First-Principles calculations to investigate the refractive index and optical dielectric constant of Na_3SbX_4 (X = S, Se) ternary chalcogenides. Phys Status Solidi 2019;256:1900131–4.
[66] Penn DR. Wave-number-Dependent dielectric function of semiconductors. Phys Rev 1962;128:2093.
[67] Hassan M, Arshad I, Mahmood Q. Computational study of electronic, optical, and thermoelectric properties of X_3PbO (X = Ca, Sr, Ba) anti-perovskites. Semicond Sci Technol 2017;32:115002.
[68] Bobrov VB, Trigger SA, van Heijst GJF, Schram PPJM. Kramers-Kronig relations for the dielectric function and the static conductivity of Coulomb systems. EPL 2010;90:10003.
[69] Wang HC, Pistor P, Marques MAL, Botti S. Double perovskites as p-type conducting transparent semiconductors: a high-throughput search. J Mater Chem 2019;7:14705.
[70] Mahmood Q, Zelai T, Usman T, Al-Qaisi S, Morsi M, Albalawi H, et al. First-principles study of lead-free double perovskites $K_2Pt(Cl/Br)_6$ for optoelectronic and renewable energy applications. J Solid State Chem 2021;301:122294.
[71] Flemban TH, Singaravelu V, Devi AAS, Roqan IS. Homogeneous vertical ZnO nanorod arrays with high conductivity on an in situ Gd nanolayer. RSC Adv 2015;5(115):94670–8.
[72] Mahmood Q, Alhossainy MH, Rashid MS, Flemban TH, Althib H, Alshahrani T, et al. First-principles study of lead-free double perovskites Rb2TeX6 (X =Cl, Br, and I) for solar cells and renewable energy. Mater Sci Eng, B 2021;266:115064.
[73] Tayebi N, Bidai K, Ameri M, Amel S, Ameri I, Al-Douri Y, et al. Pressure and temperature dependence of the structural, elastic, and thermodynamic properties of potassium telluride: first-principles calculations. Chin J Phys 2017;55:769–79.
[74] Litimein F, Khenata R, Bouhemadou A, Al-Douri Y, Bin Omran S. First-principle calculations to investigate the elastic and thermodynamic properties of RBRh3 (R = Sc, Y and La) perovskite compounds. Mol Phys 2012;110:121–8.
[75] Moulay N, Ameri M, Azaz Y, Zenati A, Al-Douri Y, Ameri I. Predictive study of structural, electronic, magnetic and thermodynamic properties of $XFeO_3$ (X = Ag, Zr and Ru) multiferroic materials in cubic perovskite structure: first-principles calculations. Materials Science-Poland 2015;33:402–13.
[76] Ayad M, Belkharroubi F, Boufadi FZ, Khorsi M, et al. First-principles calculations to investigate magnetic and thermodynamic properties of new multifunctional full-Heusler alloy Co_2TaGa. Indian J Phys 2020;94:767–77.
[77] Sajjad M, Singh N, Sattar S, De Wolf S, Schwingenschlogl U. Ultralow lattice thermal conductivity and thermoelectric properties of monolayer Tl2O. ACS Appl Energy Mater 2019;2:3004–8.
[78] Sajjad M, Mahmood Q, Singh N, Andreas Larsson J. Ultralow lattice thermal conductivity in double perovskite Cs_2PtI_6: a promising thermoelectric material. ACS Appl Energy Mater 2020;3(11):11293–9.
[79] Zhou G, Wang D. Few-quintuple Bi_2Te_3 nanofilms as potential thermoelectric materials. Sci Rep 2015;5(1):8099.
[80] Campi D, Paulatto L, Fugallo G, Mauri F, Bernasconi M. First-Principles calculation of lattice thermal conductivity in crystalline phase change materials: GeTe, Sb_2Te_3, and $Ge_2Sb_2Te_5$. Phys Rev B 2017;95(2):024311.
[81] Li W, Carrete J, Katcho NA, Mingo N. ShengBTE: A Solver of the Boltzmann Transport Equation for Phonons. Comput Phys Commun 2014;185:1747–58.